Adsorption behavior of phosphate on Mg–Al layered double hydroxide/montmorillonite composite

Yongzai Wang[a,]*, Gongshen Li[b]

[a]*Center of Analysis and Testing, Shandong University of Technology, Zibo, Shandong 255049, P.R. China,*
Tel./Fax: +86 0533 2786781; email: yzwang@sdut.edu.cn
[b]*College of Science, Shandong University of Technology, Zibo, Shandong 255049, P.R. China, Tel./Fax: +86 0533 2782308;*
email: ligs@sdut.edu.cn

ABSTRACT

In this study, Mg–Al-layered double hydroxide (LDH) and montmorillonite (M) were mixed (mass ratio = 1:1) with high-shear action to prepare a mineral composite (LDH–M). The structure, morphology, and textural properties of LDH and LDH–M were investigated via X-ray diffraction, field-emission scanning electron microscopy, Fourier transform infrared spectroscopy, and nitrogen physisorption. The phosphate adsorption performances of LDH and LDH–M were assessed and compared by conducting batch experiments. The effects of initial adsorbate concentration and contact time on phosphate uptake were examined. The adsorption kinetics and isothermal adsorption of both adsorbents showed that the pseudo-second-order model and the Langmuir isotherm fitted well with the experimental data. The maximum adsorption capacity of 127.8 mg g^{-1} of phosphate onto LDH–M improved by ~21% compared with that onto pure LDH. Hence, the composite exhibited better affinity toward phosphate adsorption than pure LDH. The enhanced adsorption of phosphate by LDH–M probably resulted from the textural changes of the composite compared with those of its precursors. The adsorption process mainly follows ion-exchange mechanism. The results revealed a synergic effect between LDH and M during phosphate removal.

Keywords: Layered double hydroxides; Montmorillonite; Composite; Phosphate; Sorption

1. Introduction

Phosphorus (P) mainly occurs as phosphate in aquatic systems. Extensive human activities, such as over application of agricultural fertilizers, detergent and paint manufacturing, mineral processing, and household applications, cause the release of large amounts of phosphate-bearing water to aquatic environments, thus resulting in eutrophication and posing a threat to humans and ecosystems. Consequently, removing phosphate from or reducing its concentration in wastewater before such water is discharged into natural water bodies is an important issue.

Different physicochemical technologies, including sorption [1,2], chemical precipitation [3], biological methods [4], and reverse osmosis [5], have been developed to reduce phosphate concentration in wastewater. Adsorption methods are widely accepted because they have the advantages of low cost, easy operation, high uptake capacity in dilute solutions, less sludge production, and few disposal problems [1].

*Corresponding author.

Many inorganic materials, such as fly ash [6], aluminum oxide [7], iron oxide [8], zirconium oxide [9], layered double hydroxides (LDHs or anionic clay) and their calcined products [1,10–12], bentonite [13], red mud [14], and zeolites [15], have been investigated for removing phosphate from wastewater. However, these single-component adsorbents exhibit varied sorption behaviors and removal efficiencies. Developing adsorbents with high uptake and fast adsorption kinetics toward phosphate removal is necessary. Composite adsorbents consisting of more than one kind of material have attracted considerable research interest in recent years. Multi-component adsorbents, such as Fe–Mn binary oxides [16], mixed Al–Fe binary hydr (oxide) [17,18], Fe–Zr binary oxide [19,20], TiO_2–Fe_2O_3 [21], zero-valent iron–Fe_3O_4 nanocomposites [22], and the mineral mixture of kaolinite–birnessite [23], have been prepared. These composite adsorbents exhibit enhanced uptake capacity and good selectivity compared with those of single-component sorbents during adsorption.

LDHs have been widely used as environmental adsorbents because of their high anion-exchange capacity and large surface area. Montmorillonite hardly sorbs anions [24]. Several groups have reported LDH- or montmorillonite-based composites as anion adsorbents. For example, some authors [25] claimed that LDHs dispersed on suitable support materials can enhance adsorption capacity toward fluoride by four to five times. Reports on the sorption characteristics of anionic clay–alginate composites indicated that these substances exhibit high uptake behavior in water treatment [26]. Montmorillonite/Fe–Al composite is effective for purifying phosphate at low concentrations under a wide range of physicochemical conditions [27]. Zr-modified MgFe–LDH(CO_3), a composite of MgFe–LDH with amorphous zirconium hydroxide, shows greater uptake of phosphate ions in P-enriched seawater than amorphous zirconium oxide and MgFe–LDH(CO_3) [10]. These findings demonstrate that LDH- or montmorillonite-based composite adsorbents exhibit different sorption behaviors toward anion removal compared with their corresponding single-component sorbents.

The objective of this study is to uniformly disperse Mg/Al LDH on the surface of montmorillonite to enhance the adsorption characteristics of Mg/Al LDH. To this end, we prepared LDH/ montmorillonite composite for the first time by high-shear dispersion technology. With the action of strong shear forces, fragmentation and disruption of the aggregation state between the precursor particles leads to the rearrangement of Mg/Al LDH and montmorillonite particles. The as-prepared composite materials were character-

ized in detail by X-ray diffraction (XRD), Fourier transform infrared (FTIR) spectroscopy, field-emission scanning electron microscopy (FESEM), and nitrogen sorption analysis, and were examined for phosphate removal in aqueous solutions through batch adsorption experiments.

2. Materials and methods

2.1. Mg/Al LDH and montmorillonite

Mg/Al LDH (hereafter referred to as LDH) were synthesized by applying the common co-precipitation method as follows: 0.075 mol Mg $(NO_3)_2 \cdot 6H_2O$ and 0.025 mol Al $(NO_3)_3 \cdot 9H_2O$ were dissolved in 150 ml of deionized water, thus forming a mixture solution. The solution was added dropwise into 50 ml of 2-M NaOH solution under vigorous stirring. The reaction mixture was heated at 60°C for 3 h for aging. The entire reaction process was decarbonated by continuous bubbling with nitrogen gas. The obtained precipitates were centrifuged, washed with decarbonated water, and vacuum dried at 110°C overnight.

The montmorillonite (hereafter abbreviated as M) used in this work was a commercial product (Yu Hong Clay Chemical Corporate, Zhejiang, China) with the following chemical composition: 63.52% SiO_2, 19.49% Al_2O_3, 1.24% Fe_2O_3, 2.42% MgO, 1.01% CaO, 1.23% K_2O, and 2.69% Na_2O. The sample has a cationic exchange capacity of 102.5 meq/100 g and contains less than 5% non-clay minerals (mainly cristobalite). The sample was used as received without further purification.

2.2. Preparation of LDH–M composite

In a typical synthesis, 1.0 g of LDH and 1.0 g of M were mixed in a glass flask that contained 200 ml of freshly decarbonated water, and stirred by a high-shear dispersing emulsifier (FA25–25A, Fluko, Shanghai, China) at 10,000 rpm for 60 min. The obtained colloidal dispersions were separated by centrifugation and vacuum dried at 80°C overnight. The resulting composite was used for subsequent adsorption studies. The as-obtained composite is denoted as LDH–M.

2.3. Characterization

The XRD patterns of the samples before and after adsorption were recorded on a Bruker D8 Advance diffractometer with the following parameters: Cu Kα radiation, 40 kV/40 mA, step size 0.02°, time for step 0.5 s. All measurements were performed on disoriented powder samples.

A field-emission scanning electron microscope (Sirion 200, FEI) was employed to observe the morphologies of the obtained samples.

FTIR spectra were obtained on a Nicolet 5700 FTIR spectrometer (resolution of 4 cm^{-1}, KBr-pressed disk technique).

The textural properties of the samples were estimated by performing nitrogen sorption experiments. The adsorption/desorption isotherms of nitrogen at 77 K were measured with an automated Micromeritics ASAP 2020 apparatus. Prior to measurements, the samples were degassed for 4 h at 120°C to remove physisorbed water molecules. Specific surface areas were determined from the Brunauer–Emmett–Teller (BET) equation. Total pore volumes were calculated using the Barret–Joyner–Halender (BJH) model based on the desorption branch of the isotherms.

2.4. Phosphate sorption experiments

Stock phosphate solution with a concentration of 500 mg l^{-1} in P was prepared by dissolving K$_2$HPO$_4$ in deionized water. The stock solution was diluted to prepare phosphate solutions with desired concentrations for the subsequent batch of adsorption experiments. Both LDH and the as-prepared composite LDH–M were used as adsorbents to compare their phosphate adsorption behaviors.

All adsorption experiments were performed in 100-ml stoppered conical flasks. The flasks were placed in a thermostatic shaking water bath, and the reaction temperature was maintained at 25°C. The pH value of the mixed solution was not adjusted and was measured as near neutral.

The phosphate concentrations in the aqueous solutions after adsorption were determined by a Dionex DX-2000 ion chromatography system equipped with an electrochemical detector and an IonPac AS18 (4 mm × 250 mm) column. The mobile phase was a 35 mM KOH solution. The determination limit of the analytical method was 0.01 mg P l^{-1}.

In the isotherm experiments, sorbent with a mass of 0.1 g was added into 50 ml phosphate solutions with various initial concentrations ranging from 50 to 200 mg l^{-1}. The mixtures were shaken for 24 h to attain equilibrium. The phosphate concentrations in the supernatant solutions separated by centrifugation were determined.

In the kinetic experiments, 50 ml of 100 mg l^{-1} phosphate solution was contacted with 0.1 g of sorbent. The mixed solution was shaken and then separated at different time intervals to collect the filtrates and residual solids. The phosphate concentrations in the filtrates were measured. Phosphate uptake by the

sorbent and its removal efficiency were, respectively, calculated with the Eqs. (1) and (2).

$$q_t = (C_0 - C_t)V/m \tag{1}$$

$$\eta = (C_0 - C_e)/C_0 \times 100\% \tag{2}$$

where q_t (mg g^{-1}) is the amount of phosphate adsorbed onto the adsorbent at time t; C_0 and C_e (mg l^{-1}) are the initial and equilibrium phosphate concentrations in the solution, respectively; C_t (mg l^{-1}) is the phosphate concentration in the solution at time t; V (l) is the volume of the solution; and m (g) is the sorbent mass.

3. Results and discussion

3.1. XRD analysis

The XRD patterns of LDH, M, and the LDH–M composite are shown in Fig. 1. The profile of the as-prepared LDH sample shows three main reflections, and the first (0 0 l) reflection was observed at d$_{003}$-value = 7.6099 Å, $2\theta = 11.321°$. All the reflections of LDH were indexed as Mg–Al LDH (PDF No. 01-070-2151). The d$_{003}$-value, i.e. the basal spacing of the LDH-layered structure, indicated the interlayer ions are NO$_3^-$ [28]. The XRD patterns of M show four main reflections, and the first (0 0 l) reflection for M was observed at d$_{001}$-value = 15.0112 Å, $2\theta = 5.883°$, which
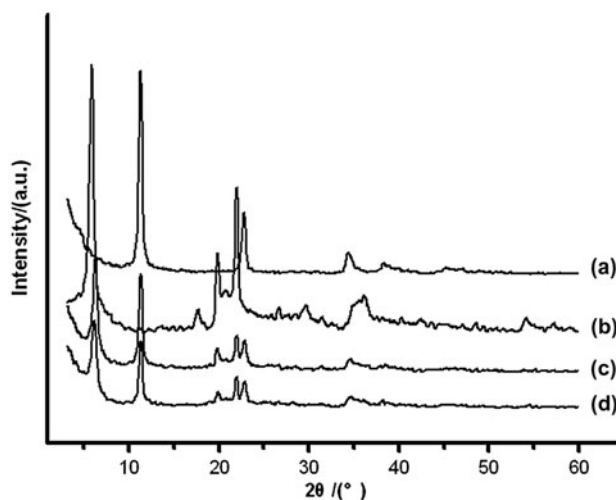

Fig. 1. XRD patterns of the adsorbents: (a) LDH, (b) M, (c) LDH–M before adsorption, and (d) LDH–M after adsorption.

characterizes the samples mainly as montmorillonite. In addition, there is reflection associated with cristobalite (d-value = 4.0395 Å, 2θ = 21.986°). All the diffraction peaks of the composite sample can be identified as LDH and M. The position and intensity of (0 0 l) reflections of LDH and M in LDH–M were not affected, thus indicating that the structure of the virgin materials was not damaged during the strong shear action. No other phase could be observed, which suggested the absence of chemical reaction among the components during mixing. Therefore, the resulting composite LDH–M is a physical mixture of LDH and M.

The basal spacing that corresponded to LDH and M in the composite exhibited no discernible change after phosphate adsorption. In general, M hardly sorbs phosphates by chemisorption, thus indicating no change in its XRD pattern. Previous studies did not show any change in the basal spacing of LDH upon interlayer exchange of nitrate with phosphate [29,30]. Therefore, the results of the current study indicate that phosphate adsorption by the composite mainly follows the ion-exchange mechanism.

3.2. FTIR spectroscopy analysis

The FTIR spectra of the composite before and after phosphate sorption are shown in Fig. 2. In the original LDH–M spectra, the sharp band at 1,384 cm^{-1} is caused by the interlayer of NO_3^- ions in pure LDH; meanwhile, the strong bands at 1,106 and 1,036 cm^{-1} can be ascribed to the symmetric and unsymmetric Si–O stretching vibration of M [31]. An intense broad band at approximately 3,494 cm^{-1} is attributed to OH-stretching vibration from the hydroxide layers and the interl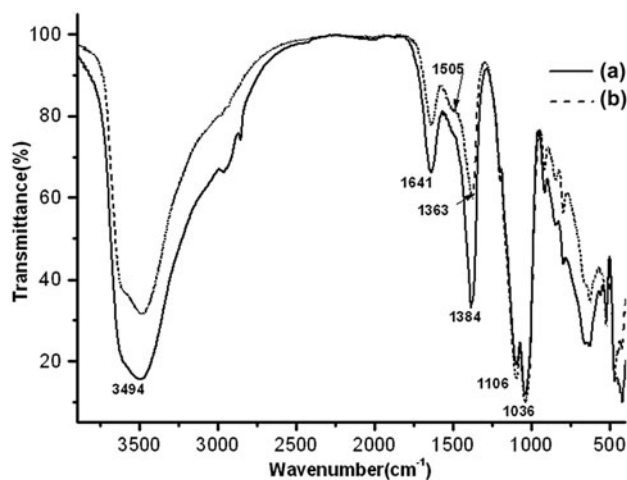ayer water in the component adsorbents. The bending vibration of water molecules is responsible for the weak band close to 1,641 cm^{-1}.

Compared with the FTIR spectra of the virgin composite sorbent, a remarkable difference was observed after phosphate sorption [Curve (2) of Fig. 2]. The band at 1,384 cm^{-1} disappeared, and a band at 1,363 cm^{-1} with a shoulder at 1,505 cm^{-1} appeared. The two new bands can be attributed to the stretching vibration of physisorbed carbonate ion in the sorbent, which probably resulted from the contamination by atmospheric CO_2 during adsorption.

The intensity of the bands at 1,106 and 1,036 cm^{-1} clearly increased after phosphate sorption. Previous literature has reported that phosphate can cause strong P–O absorptions at 1,106 and 1,036 cm^{-1}, similar to those of Si–O vibration in M [31,32]. Enhancement of the intensity of the LDH–M bands at 1,106 and 1,036 cm^{-1} after phosphate sorption is probably caused by overlapping peaks of P–O and Si–O vibrations. This result, as well as the absence of a nitrate group band, provides strong evidence for the complete replacement of interlayer nitrate ions in LDH with phosphate ions.

3.3. FESEM observation

Representative FESEM images of the adsorbents are shown in Fig. 3. The morphologies of LDH and M are small round plates (30–50 nm in diameter) and irregular large thin flakes, respectively. The image of the as-prepared composite showed tiny LDH particles that are well distributed over the large surface of M, thus, demonstrating that intensive shearing action during preparation results in the formation of a uniform mixture of the composite.

The image showed that the particles of the composite did not change their morphologies and the surface appeared to be looser after phosphate adsorption. Many inter-particle or intra-particle voids were generated in the sample during adsorption.

3.4. BET and pore size analysis

The BET surface areas and pore volumes of M, LDH, and LDH–M are summarized in Table 1. As shown in Fig. 4, all adsorbents display similar N$_2$ adsorption–desorption isotherms and exhibit an H3 hysteresis loop ascribed to inter-particle pores. The figure shows that LDH–M has a higher pore volume than M and LDH. Pores may be formed by the aggregation of various flake-like M particles and LDH plate particles. The BET surface area of the composite

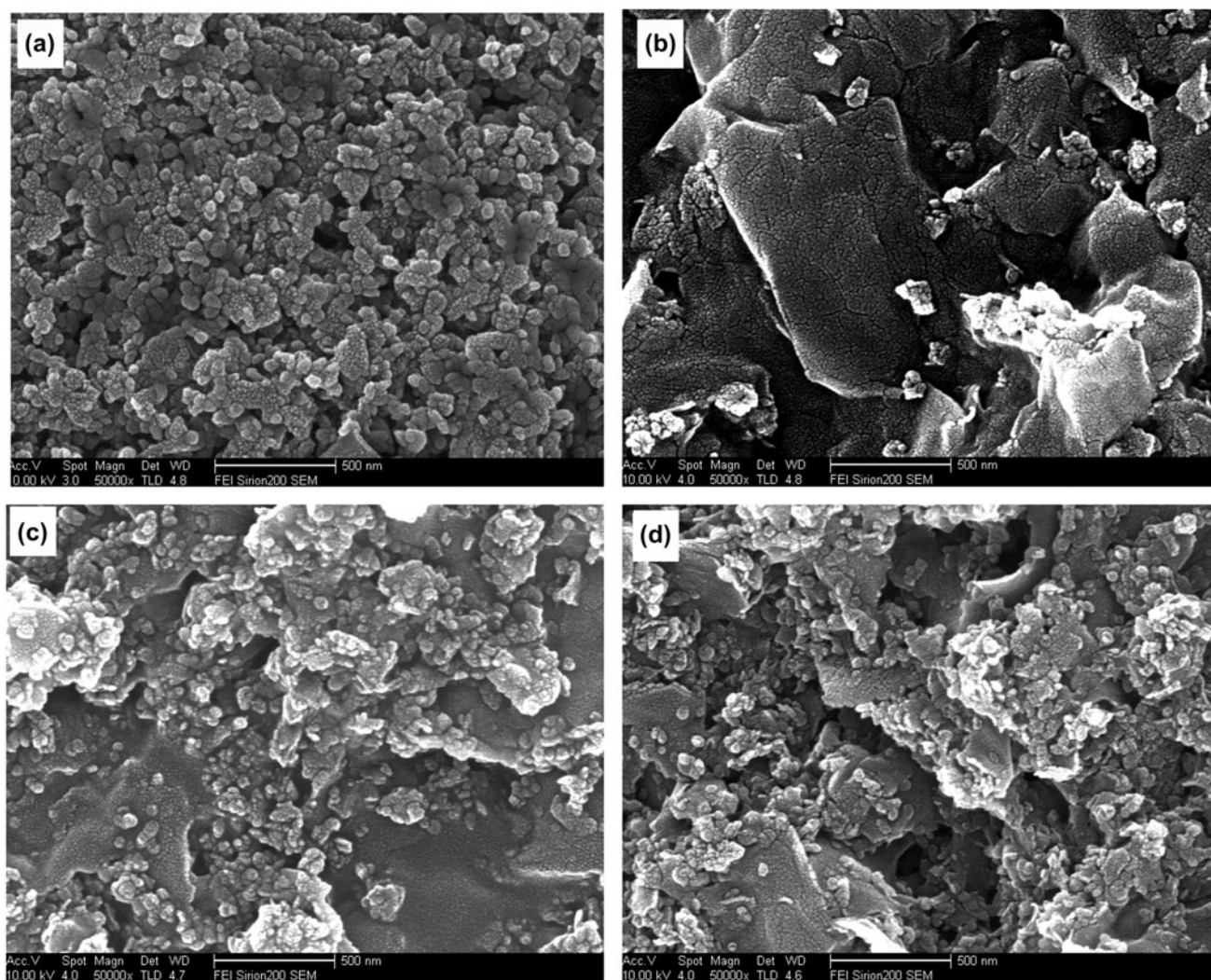Fig. 2. The FTIR spectra of LDH–M (a) before and (b) after adsorption.

Fig. 3. FESEM images of the adsorbents: (a) LDH, (b) M, (c) LDH-M before adsorption, and (d) LDH-M after adsorption.

Table 1
Textural parameters for adsorbents

	LDH	M	LDH–M
S_{BET} (m^2 g^{-1})	104.2	30.2	60.9
Total pore volume (cm^3 g^{-1})	0.26	0.11	0.30

is approximately the average of those of M and LDH, but its total pore volume is higher than those of its constituents. The change in textural properties can be attributed to the rearrangement of the virgin particles during mixing, which is in accordance with previous FESEM observation.

The BJH pore size distribution plot demonstrated that the composite has a bimodal distribution of pores. The peak for the first narrow distribution is centered at 4.4 nm. The second distribution is within the range of 4.8–45.5 nm, which represents the majority of the pores, and exhibits a maximum value at approximately 27.1 nm. Small pores may have originated from the inherent mesoporosity of M or LDH whereas large pores at various sizes resulted from composite formation. A similar observation has been reported for Mg/Al LDH–alginate composite [26]. Such pore features may be beneficial to trapping and adsorbing phosphate during adsorption.

3.5. Sorption isotherms

Equilibrium data for phosphate adsorption were analyzed to determine the adsorption capacity of the sample by considering the Langmuir and Freundlich isotherm models.
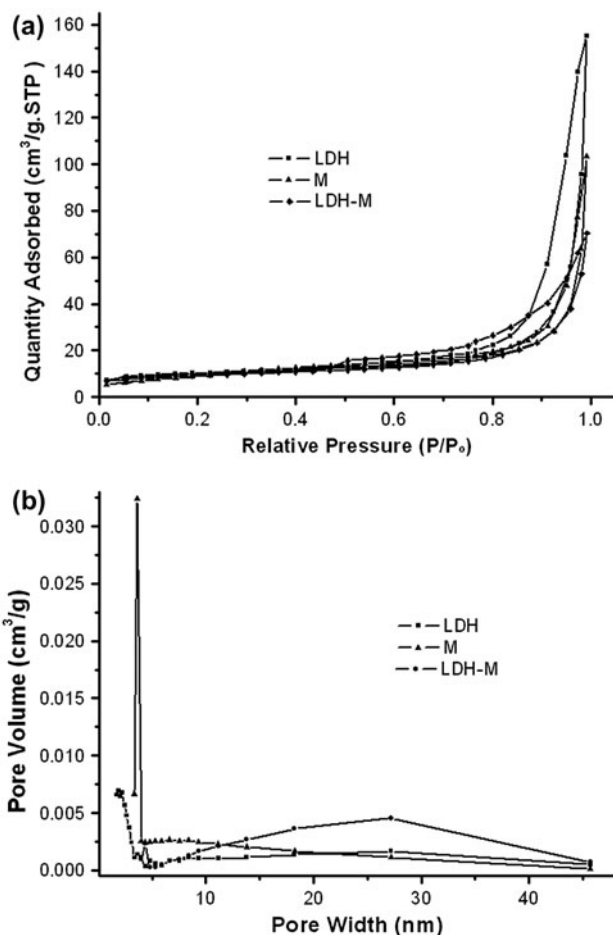
Fig. 4. (a) N_2 adsorption–desorption isotherms and (b) pore size distribution of the adsorbents.

and n are the Freundlich constants that correspond to adsorption capacity and adsorption intensity, respectively. Small n values typically indicate a heterogeneous surface.

The adsorption results of phosphate on LDH and LDH–M are shown in Fig. 5. All curves exhibited a similar trend, with q_e increasing rapidly during the initial stages and gradually decreasing with increasing C_e. This trend can be attributed to the less adsorption sites available for fixed adsorbent loading when high phosphate concentrations were used.

The fitted results for the Langmuir and Freundlich models are reported in Fig. 6 and Table 2. According to the correlation coefficient R^2, the experimental data can be fitted well by the Langmuir model rather than by the Freundlich model, thus indicating that adsorption is a monolayer and occurs homogeneously on the surface of the adsorbents. The Langmuir binding constant b increased in the order of LDH–M > LDH, thus exhibiting an increase in relative phosphate-bonding strength with the adsorbents. The n value follows the order of LDH–M < LDH, thus demonstrating that the involved binding sites are more heterogeneous in the composite than in the single-component LDH.

As shown in Table 2, the calculated q_m followed the order of LDH–M > LDH. The maximum phosphate uptake by LDH–M was 127.76 mg g^{-1}, which was approximately 21% higher than that of LDH. The phosphate adsorbed by the composite adsorbent is also higher than those of most LDH materials reported in literature [1]. Previous result reveals that the phosphate adsorption capacity of M is negligible [24]. Hence, the presence of M in the

The Langmuir model presumes no interaction among adsorbed molecules, and that the adsorbate is distributed in a homogeneous monolayer within the adsorbent. The Freundlich model describes an adsorbent with a heterogeneous surface and implies multilayer sorption. The linear forms of the Langmuir and Freundlich models are, respectively, represented by Eqs. (3) and (4):

$$C_e/q_e = C_e/q_m + 1/(q_m b) \qquad (3)$$

$$\log q_e = \log K_f + (1/n)\log C_e \qquad (4)$$

where C_e and q_e are the equilibrium adsorbate concentrations in the solution (mg l^{-1}) and on the adsorbent (mg g^{-1}), respectively; q_m is the maximum adsorption capacity (mg g^{-1}); b is the Langmuir constant related to the sorption energy (l mg^{-1}); and K_f
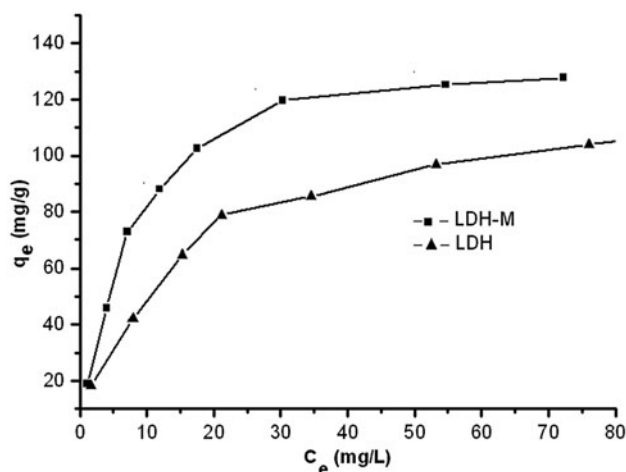

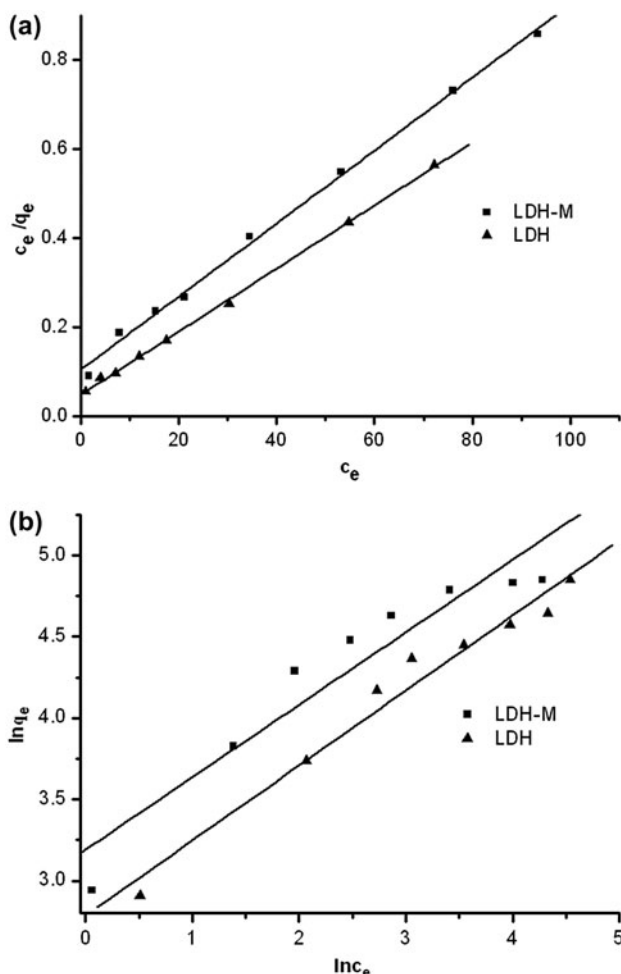Fig. 5. Adsorption isotherms of phosphate by the adsorbents.

Fig. 6. (a) Linear Langmuir adsorption isotherm and (b) linear Freundlich adsorption isotherm.

composite significantly enhances phosphate adsorption by LDH, and indicates that the mixed composite adsorbent exhibits higher adsorption capacity toward phosphate removal than single-component adsorbents. Similar observations have been reported on the adsorption behaviors of other composite sorbents, such as Fe–Fe$_3$O$_4$ nanocomposite [22], kaolinite–birnessite mixture system [23], and anionic clay–alginate composites [26].
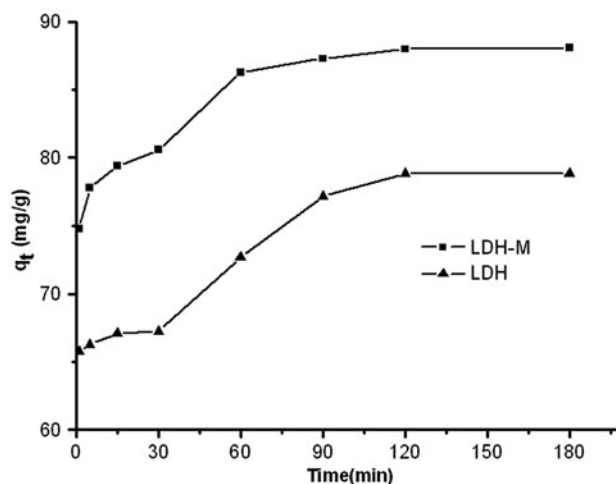

Fig. 7. Effect of contact time on phosphate adsorption onto LDH–M and LDH.

A large enhancement in phosphate adsorption capacity for LDH–M may be related to its textural features. The increased pore volume in the composite can enhance possible accessible diffusion pathways and allow more phosphate ions to access the adsorbent easily [13]. Hence, the as-synthesized composite is regarded as a superior phosphate adsorbent relative to single-component adsorbents.

3.6. Adsorption kinetics

A plot of the amount of phosphates adsorbed by LDH and LDH–M vs. contact time is shown in Fig. 7. Phosphate uptake on the adsorbents increased with time and reached equilibrium at approximately 3 h (Fig. 7). Most phosphates are removed by LDH–M during the first 60 min of adsorption compared with 120 min by LDH.

Phosphate removal efficiencies within 3 h are 78.8 and 88.3% using LDH and LDH–M, respectively. Phosphate removal by LDH–M is more efficient than that by pure LDH.

Table 2
Langmuir and Freundlich isotherm parameters for phosphate adsorption on the adsorbents

Adsorbent	Langmuir				Freundlich		
	q_m (mg g^{-1})	b (l mg^{-1})	R^2		K_f (mg g^{-1})	n	R^2
LDH	105.68	0.078	0.9981		16.86	2.26	0.9783
LDH–M	127.76	0.154	0.9995		24.32	2.24	0.9533

Table 3
Kinetic parameters for phosphate adsorption on adsorbents

Sorbent	Pseudo-first-order		Pseudo-second-order	
	k_1 (min^{-1})	R^2	k_2 (mg (g min)$^{-1}$) $\times 10^{-3}$	R^2
LDH	0.023	0.9490	3.6	0.9990
LDH–M	0.025	0.9866	9.0	0.9998

To evaluate the mechanism of phosphate adsorption, kinetic data were fitted by the classical pseudo-first rate and pseudo-second rate equations (Eqs. (5) and (6)).

$$\log(q_e - q_t) = \log q_e - (k_1 t/2.303) \qquad (5)$$
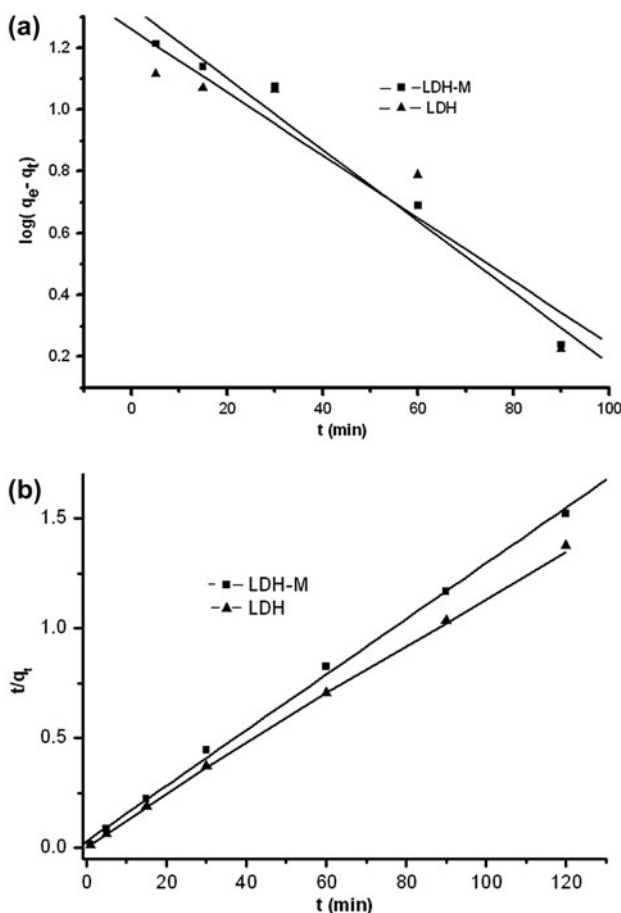
$$t/q_t = 1/(k_2 q_e^2) + t/q_e \qquad (6)$$

where q_t (mg g^{-1}) is the adsorbed amount at time t; q_e (mg g^{-1}) is the adsorbed amount at equilibrium; and k_1 (min^{-1}) and k_2 [mg (g min)$^{-1}$] are the equilibrium rate constants of the pseudo-first and pseudo-second order models, respectively.

The linear plots of $\log(q_e - q_t)$ vs. t (Fig. 8(a)) and t/q_t vs. t (Fig. 8(b)) give their respective kinetic parameters (Table 3). Based on the regression coefficient R^2, the pseudo-second-order model is in best agreement with the kinetic data for both adsorbents, thus indicating that the rate-limiting adsorption step is probably chemisorption between the adsorbent and the adsorbate [33]. This is in accordance with the results derived from XRD and FTIR analyses, which indicate that phosphate adsorption by LDH–M mainly follows ion-exchange mechanism.

Table 3 shows that the rate constant k_2 of the composite is higher than that of LDH. The increase in the k_2 value of LDH–M may be attributed to the increased number of approachable pore sites in the composite adsorbent. This result is consistent with other reports on phosphate adsorption [10,25,26] and demonstrates the advantage of the composite.

4. Conclusion

A high-shear dispersing method has been successfully applied to prepare a novel LDH–M composite. Dispersed LDH particles are uniformly loaded on the surface of montmorillonite in the composite. The composite possesses bimodal mesopores and enhanced porosity. Phosphate adsorption on both LDH and LDH–M can be satisfactorily fitted by pseudo-second-order kinetics, and data agree well with the Langmuir adsorption isotherm model. The maximum adsorption capacity of phosphate onto LDH–M is improved by ~21% compared with that of pure LDH. The increased uptake of LDH–M can be attributed to the increase in total pore volume of the composite, which results from the rearrangement of the virgin particles during shear action. The composite material is considered as a low-cost and effective adsorbent for removing phosphate from aqueous solutions.

Fig. 8. Kinetic plots of phosphate adsorption onto adsorbents: (a) the pseudo-first-order model and (b) the pseudo-second-order model.

Acknowledgments

References

[1] K.H. Goh, T.T. Lim, Z. Dong, Application of layered double hydroxides for removal of oxyanions: A review, Water Res. 42 (2008) 1343–1368.

[2] E.N. Peleka, E.A. Deliyanni, Adsorptive removal of phosphates from aqueous solutions, Desalination 245 (2009) 357–371.

[3] M.I. Aguilar, J. Saez, M. Llorens, A. Soler, J.F. Ortuno, Nutrient removal and sludge production in the coagulation–flocculation process, Water Res. 36 (2002) 2910–2919.

[4] T. Mino, M.C.M. van Loosdrecht, J.J. Heijnen, Microbiology and biochemistry of the enhanced biological phosphate removal process, Water Res. 32 (1998) 3193–3207.

[5] E.M. van Voorthuizen, A. Zwijnenburg, M. Wessling, Nutrient removal by NF and RO membranes in a decentralized sanitation system, Water Res. 39 (2005) 3657–3667.

[6] S.G. Lu, S.Q. Bai, L. Zhu, H.D. Shan, Removal mechanism of phosphate from aqueous solution by fly ash, J. Hazard. Mater. 161 (2009) 95–101.

[7] H.P. Grigoropoulou, D.A. Georgantas, Orthophosphate and metaphosphate ion removal from aqueous solution using alum and aluminum hydroxide, J. Colloid Interface Sci. 315 (2007) 70–79.

[8] L. Zeng, X. Li, J. Liu, Adsorptive removal of phosphate from aqueous solutions using iron oxide tailings, Water Res. 38 (2004) 1318–1326.

[9] H.L. Liu, X.F. Sun, C.Q. Yin, C. Hu, Removal of phosphate by mesoporous ZrO_2, J. Hazard. Mater. 151 (2008) 616–622.

[10] R. Chitrakar, S. Tezuka, J. Hosokawa, Y. Makita, A. Sonoda, K. Ooi, T. Hirotsu, Uptake properties of phosphate on a novel Zr–modified MgFe–LDH(CO_3), J. Colloid Interface Sci. 349 (2010) 314–320.

[11] Y. Xu, Y. Dai, J. Zhou, Z.P. Xu, G.R. Qian, G.Q.M. Lu, Removal efficiency of arsenate and phosphate from aqueous solution using layered double hydroxide materials: intercalation vs. precipitation, J. Mater. Chem. 20 (2010) 4684–4691.

[12] H. He, H. Kang, S. Ma, Y. Bai, X. Yang, High adsorption selectivity of ZnAl layered double hydroxides and the calcined materials toward phosphate, J. Colloid Interface Sci. 343 (2010) 225–231.

[13] M. Zamparas, A. Gianni, P. Stathi, Y. Deligiannakis, I. Zacharias, Removal of phosphate from natural waters using innovative modified bentonites, Appl. Clay Sci. 62–63 (2012) 101–106.

[14] S.B. Wang, W.W. Huang, Z.H. Zhu, L. Li, X.D. Yao, V. Rudolph, F. Haghseresht, Phosphate removal from wastewater using red mud, J. Hazard. Mater. 158 (2008) 35–42.

[15] D. Wu, B. Zhang, C. Li, Z. Zhang, H. Kong, Simultaneous removal of ammonium and phosphate by zeolite synthesized from fly ash as influenced by salt treatment, J. Colloid Interface Sci. 304 (2006) 300–306.

[16] G.S. Zhang, H.J. Liu, R.Q. Liu, J.H. Qu, Removal of phosphate from water by a Fe–Mn binary oxide adsorbent, J. Colloid Interface Sci. 335 (2009) 168–174.

[17] O.R. Harvey, R.D. Rhue, Kinetics and energetics of phosphate sorption in a multi-component Al(III)–Fe(III) hydr(oxide) sorbent system, J. Colloid Interface Sci. 322 (2008) 384–393.

[18] H.J. Hong, W. Farooq J.-S. Yang, J.W. Yang, Preparation and evaluation of Fe-Al binary oxide for arsenic removal: Comparative study with single metal oxides, Sep. Sci. Technol. 45 (2010) 1975–1981.

[19] F. Long, J.L. Gong, G. Zeng, L. Chen, X.Y. Wang, J.H. Deng, Q.Y. Niu, H.Y. Zhang, X.R. Zhang, Removal of phosphate from aqueous solution by magnetic Fe–Zr binary oxide, Chem. Eng. J. 171 (2011) 448–455.

[20] Z. Ren, L. Shao, G. Zhang, Adsorption of phosphate from aqueous solution using an iron–zirconium binary oxide sorbent, Water Air Soil Pollut. 223 (2012) 4221–4231.

[21] M. D'Arcy, D. Weiss, M. Bluck, R. Vilar, Adsorption kinetics, capacity and mechanism of arsenate and phosphate on a bifunctional TiO_2–Fe_2O_3 bi-composite, J. Colloid Interface Sci. 364 (2011) 205–212.

[22] X. Lv, J. Xu, G. Jiang, J. Tang, X. Xu, Highly active nanoscale zero-valent iron (nZVI)–Fe_3O_4 nanocomposites for the removal of chromium(VI) from aqueous solutions, J. Colloid Interface Sci. 369 (2012) 460–469.

[23] Y. Arai, Aqueous interfacial chemistry of kaolinite for the removal of Cu(II) in the presence of birnessite: Kinetic and spectroscopic studies, Appl. Clay Sci. 53 (2011) 572–580.

[24] F. Haghseresht, S.B. Wang, D.D. Do, A novel lanthanum-modified bentonite, Phoslock, for phosphate removal from wastewaters, Appl. Clay Sci. 46 (2009) 369–375.

[25] N. Viswanathan, S. Meenakshi, Selective fluoride adsorption by a hydrotalcite/chitosan composite, Appl. Clay Sci. 48 (2010) 607–611.

[26] S. Mandal, V.S. Patil, S. Mayadevi, Alginate and hydrotalcite-like anionic clay composite systems: Synthesis, characterization and application studies, Microporous Mesoporous Mater. 158 (2012) 241–246.

[27] M.X. Zhu, K.Y. Ding, S.H. Xu, X. Jiang, Adsorption of phosphate on hydroxyaluminum- and hydroxyiron-montmorillonite complexes, J. Hazard. Mater. 165 (2009) 645–651.

[28] R.L. Frost, A.W. Musumeci, Nitrate absorption through hydrotalcite reformation, J. Colloid Interface Sci. 302 (2006) 203–206.

[29] R.L. Frost, A.W. Musumeci, M.O. Adebajo, W. Martens, Using thermally activated hydrotalcite for the uptake of phosphate from aqueous media, J. Therm. Anal. Calorim. 89 (2007) 95–99.

[30] K.S. Triantafyllidis, E.N. Peleka, V.G. Komvokis, P.P. Mavros, Iron-modified hydrotalcite-like materials as highly efficient phosphate sorbents, J. Colloid Interface Sci. 342 (2010) 427–436.

[31] M.J. Wilson, Clay Mineralogy: Spectroscopic and Chemical Determinative Methods, M.J. Wilson (Ed.), Chapman & Hall, London, 1994.

[32] L. Medvecky, T. Sopcak, J. Durisin, J. Briancin, Nanohydroxyapatite prepared from non-toxic organic Ca^{2+} compounds by precipitation in aqueous solution, Mater. Lett. 65 (2011) 3566–3569.

[33] Y.-S. Ho, Review of second-order models for adsorption systems, J. Hazard. Mater. 136 (2006) 681–689.